frontiers | Frontiers in Environmental Science

TYPE Original Research
PUBLISHED 30 September 2024
DOI 10.3389/fenvs.2024.1450485

OPEN ACCESS

EDITED BY
Divya Pal,
Stockholm University, Sweden

REVIEWED BY
Krishna Yadav,
Iowa State University, United States
Anuradha Goswami,
University of Alabama at Birmingham, United States

*CORRESPONDENCE
Ahmed Barhoum,
ahmed.barhoum@science.helwan.edu.eg

RECEIVED 17 June 2024
ACCEPTED 10 September 2024
PUBLISHED 30 September 2024

CITATION
Hemmami H, Zeghoud S, Ben Amor I, Alnazza Alhamad A, Tliba A, Alsalme A, Cornu D, Bechelany M and Barhoum A (2024) Green synthesis of CaO nanoparticles from chicken eggshells: antibacterial, antifungal, and heavy metal (Pb^{2+}, Cr^{2+}, Cd^{2+} and Hg^{2+}) adsorption properties.
Front. Environ. Sci. 12:1450485.
doi: 10.3389/fenvs.2024.1450485

Green synthesis of CaO nanoparticles from chicken eggshells: antibacterial, antifungal, and heavy metal (Pb^{2+}, Cr^{2+}, Cd^{2+} and Hg^{2+}) adsorption properties

Hadia Hemmami[1,2], Soumeia Zeghoud[1,2], Ilham Ben Amor[1,2], Ali Alnazza Alhamad[3,4], Ali Tliba[5], Ali Alsalme[6], David Cornu[7], Mikhael Bechelany[7,8] and Ahmed Barhoum[9]*

[1]Department of Process Engineering and Petrochemical, Faculty of Technology, University of El Oued, El Oued, Algeria, [2]Renewable Energy Development unit in Arid Zones (UDERZA), University of El Oued, El Oued, Algeria, [3]Department of Chemistry, Faculty of Science, University of Aleppo, Aleppo, Syria, [4]Department of Technology of organic synthesis, Ural Federal University, Yekaterinburg, Russia, [5]Laboratory Valorisation and Technology of Saharan Resources (VTRS), University of El Oued, El Oued, Algeria, [6]Department of Chemistry, College of Science, King Saud University, Riyadh, Saudi Arabia, [7]Institut Européen des Membranes (IEM), UMR 5635, University of Montpellier, ENSCM, CNRS, Montpellier, France, [8]Functional Materials Group, Gulf University for Science and Technology (GUST), Mubarak Al-Abdullah, Kuwait, [9]NanoStruc Research Group, Chemistry Department, Faculty of Science, Helwan University, Cairo, Egypt

Background: Chicken eggshells, a common poultry byproduct, are rich in calcium and provide a sustainable source for producing calcium oxide nanoparticles (CaO NPs). Their use in eco-friendly synthesis aligns with the growing emphasis on sustainable materials for environmental and biomedical applications. Objectives: This study develops an eco-friendly method for synthesizing CaO NPs from chicken eggshells, characterizes their physicochemical properties, and evaluates their antibacterial and antifungal activities. It also tests their effectiveness in removing heavy metal ions (Pb^{2+}, Cr^{2+}, Cd^{2+}, and Hg^{2+}) from aqueous solutions.

Methods: CaO NPs were synthesized by calcining chicken eggshells at 700°C for 7 h. Comprehensive characterization included analysis of crystalline structure, morphology, optical properties, bandgap energy, chemical composition, and thermal stability. Antibacterial and antifungal activities were tested using the well-agar diffusion method. Batch adsorption experiments evaluated heavy metal ion removal under varying conditions of pH, temperature, stirring time, and adsorbent concentration

Results: The synthesis produced spherical, single-crystal CaO NPs with diameters ranging from 5 to 30 nm and a crystalline size of approximately 20 nm. The nanoparticles had a bandgap energy of about 4.7 eV. Significant antibacterial activity was observed against *Staphylococcus aureus*, *Klebsiella pneumoniae*, and *Escherichia coli*, with increasing inhibition zones correlating with nanoparticle concentration. The CaO NPs also effectively inhibited *Candida albicans*. For efficient metal ion removal, the optimal conditions were found to be 30 min at pH 6 with 40 mg of CaO NPs at 25°C, achieving recovery rates of 98% for Pb^{2+}, 97% for Cd^{2+}, 97% for Cr^{2+}, and 97% for Hg^{2+}. For near-complete removal,

extending the process to 70 min at pH 6 with 40 mg of CaO NPs at 45°C achieved the highest recovery rates: 99% for Pb^{2+}, 98% for Cd^{2+}, 99% for Cr^{2+}, and 99% for Hg^{2+}, though this approach involves higher energy and cost.

Conclusion: CaO NPs derived from chicken eggshells are effective antibacterial agents and adsorbents for heavy metal removal. These findings highlight their potential for sustainable applications in environmental and biomedical fields.

KEYWORDS

biowaste utilization, eco-friendly materials, environmental remediation, wastewater treatment, heavy metal removal, nano-adsorbents, antibacterial agents

Highlights

- Green synthesis of CaO NPs from chicken eggshells by thermal annealing at 700°C.
- Significant antibacterial and antifungal activity against various pathogens demonstrated.
- Heavy metal removal of 99% achieved in solutions under optimized conditions.
- Characterization revealed high-quality, spherical CaO NPs synthesized.

1 Introduction

The increasing volume of solid waste poses a significant challenge to sustainability worldwide and its improper management exacerbates public health and environmental issues. Vast quantities of solid waste, including municipal, industrial and hazardous waste, are generated worldwide (Ferdoush et al., 2024). Food waste is a primary contributor to environmental degradation, and it is expected to increase by 44% from 2005 to 2025 (Zhang et al., 2018). Industrialization and population growth drive this surge in waste production (Aditya et al., 2021). Eggshells, sourced predominantly from households, restaurants, and bakeries, represent a significant waste item. Despite their potential for transformation into valuable products, eggshells are typically disposed of in landfills, leading to environmental problems, such as malodorous emissions and pest attraction. Eggshell recycling is a promising solution to environmental concerns and landfill overuse. Transforming eggshell waste into useful products, such as CaO nanoparticles (NPs), can contribute to sustainable waste management practices. This approach mitigates their

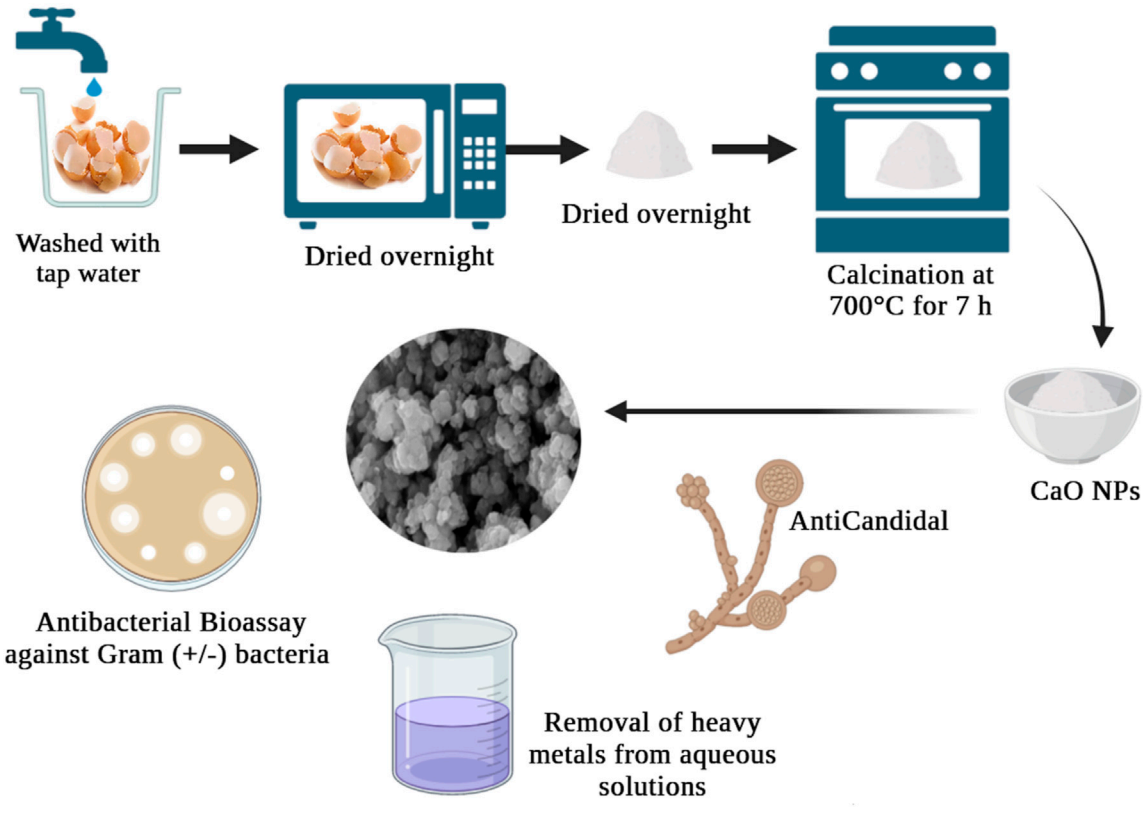

GRAPHICAL ABSTRACT

environmental impact and also supports the circular economy by converting waste into valuable resources. Recycling eggshells into CaO NPs highlights the importance of innovative recycling methods for achieving sustainability goals (Perkumienė et al., 2023; Varjani et al., 2021).

Calcium oxide (CaO), commonly known as quicklime or burnt lime, is essential across various industries including petroleum refining, biodiesel production, and water purification. Typically produced by heating $CaCO_3$ such as limestone or seashells above 825°C, CaO is a key component in many applications (Boey et al., 2011). Recent advancements have focused on CaO NPs, which are synthesised from eggshells an abundant source of $CaCO_3$ and have shown exceptional antibacterial properties against various microorganisms (Abuzeid et al., 2023). These nanoparticles are promising in medical and environmental fields, especially in combating antimicrobial resistance and biofilm-related infections (Kumari et al., 2023; Roy et al., 2013). In addition to their antimicrobial potential, CaO's versatility extends to wastewater treatment. Approximately half of the CaO produced is converted to $Ca(OH)_2$, or hydrated lime, used for disinfection and purification in wastewater management (Xiong et al., 2017). When added to wastewater, CaO raises the pH to 10.5–11.00, which helps to eliminate bacteria, viruses, and heavy metals. CaO is also crucial in drinking water treatment, where it aids in impurity removal through coagulation, precipitation, and pH adjustment, effectively neutralizing acidic waters and disinfecting by destroying pathogens (Chen et al., 2009; Kataki et al., 2021; Silva, 2023). This wide array of applications underscores CaO's critical role in ensuring clean water and advancing antimicrobial solutions.

Various chemical methods are employed to synthesize CaO NPs, each with unique advantages and challenges. Hydrothermal synthesis involves dissolving $Ca(NO_3)_2$ in deionized water, adjusting the pH with NaOH, and heating the solution in a Teflon-lined autoclave at 120°C–200°C for 6–24 h (Naz et al., 2023). This method provides precise control over nanoparticle characteristics but requires expensive equipment and extended processing times. The sol-gel method starts with dissolving a calcium precursor, such as $Ca(NO_3)_2$ or $Ca(CH_3COO)_2$, in a solvent (ethanol or water) with chelating agents to stabilize the solution. Gelation occurs by adjusting the pH with NH_4OH, resulting in a sol that ages into a gel, which is then dried and calcined at high temperatures (500°C–900°C) to form CaO NPs. Similarly, the precipitation method dissolves calcium salts like $CaCl_2$ in water and induces precipitation by adding a strong base like NaOH. The precipitate is filtered, washed, and calcined to yield CaO NPs, though this process may require extensive purification steps to remove residual chemicals. Another approach, the solvothermal method, uses organic solvents at high temperatures and pressures to control nanoparticle morphology but also demands sophisticated equipment (Andarini et al., 2021). While these methods offer versatility in tailoring particle size and crystallinity, they often involve expensive reagents, longer reaction times, and complex setups (Alobaidi et al., 2022). In contrast, thermal decomposition of a $CaCO_3$-rich source, such as eggshells, offers a more cost-effective and sustainable approach (Naz et al., 2023).

This study introduces a novel, eco-friendly method for synthesizing CaO NPs from chicken eggshells, emphasizing its sustainability and cost-effectiveness. By recycling eggshell waste, this approach not only produces valuable nanomaterials but also does so with minimal environmental impact. The synthesis method is both cost-effective and sustainable, avoiding harmful chemicals and complex procedures, and operates at a relatively low temperature sufficient to achieve the desired CaO NPs properties. This low-temperature process reduces energy consumption compared to traditional methods and involves minimal equipment and shorter processing times, making it economically viable for large-scale production. Comprehensive characterization included analysis of crystalline structure, morphology, optical properties, bandgap energy, chemical composition, and thermal stability. The study uniquely evaluates the antimicrobial properties of the CaO NPs against Gram-negative and Gram-positive bacteria, as well as *Candida* albicans, and assesses their effectiveness in removing heavy metal ions (Pb^{2+}, Cr^{2+}, Cd^{2+}, and Hg^{2+}) from aqueous solutions. Key factors influencing adsorption, such as temperature, contact time, pH, and CaO NPs dosage, were systematically explored. This research contributes to green nanotechnology by providing a sustainable solution to environmental and health challenges through the innovative use of waste materials.

2 Experimental

2.1 Materials and reagent

Chicken eggshells, discarded as waste, were collected from various sources in El Oued, Algeria (6°52′03″E, 33°22′06″N), including local restaurants, bakeries, and poultry farms. These eggshells served as the precursor for CaO NPs synthesis. Dimethyl sulfoxide (DMSO; 99%), hydrochloric acid (HCl; 99%), and sodium hydroxide (NaOH; 97%) were obtained from Biochem Chemopharma. DMSO was used as a solvent for the preparation of nanoparticle suspensions in biological assays. HCl and NaOH were employed for adjusting the pH of solutions during metal adsorption experiments. Mueller-Hinton agar, sourced from Bioscan Industrie, Algeria, was used as the growth medium for bacterial cultures during antibacterial testing. Bacterial strains, including *Pseudomonas aeruginosa* (ATCC 27853), *Klebsiella pneumoniae* (ATCC 13883), *Escherichia coli* (ATCC 25922), and *Staphylococcus aureus* (ATCC 25923), were obtained from the Algerian Culture Centre of Microorganisms and used to evaluate the antibacterial efficacy of the CaO nanoparticles. Stock solutions of heavy metal ions were prepared for adsorption studies, using chromium (II) from $CrCl_2$ (95%), mercury (II) from $HgCl_2$ (99%), cadmium (II) from $CdCl_2$ (99.9%), and lead (II) from $Pb(NO_3)_2$ (99.9%) sourced from Sigma-Aldrich. Ciprofloxacin (CIP-5), obtained from Humeau Laboratories, France, was used as a reference antibiotic for antibacterial comparison during bioassays.

2.2 CaO NP synthesis

The synthesis of CaO NPs from chicken eggshells (Figure 1) started by thoroughly washing the collected eggshells in distilled water, followed by air drying for 48 h to ensure complete moisture removal. Then, the dried eggshells were finely ground into a powder using mortar and pestle to achieve a uniform consistency. This

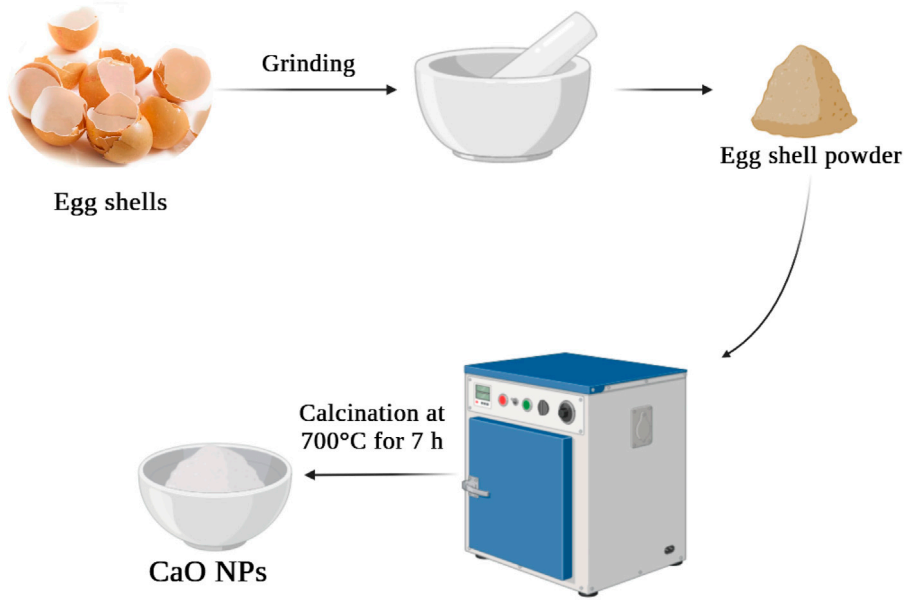

FIGURE 1
Schematic presentation showing the CaO NP synthesis starting from chicken eggshells.

powder was calcined in a furnace at 700°C in open air atmosphere for 7 h, allowing the complete decomposition of $CaCO_3$ and organic matters present in the eggshells. Throughout this process, gaseous H_2O and CO_2 were efficiently evaporated, resulting in the formation of pure CaO NPs.

2.3 CaO NP characterization

The crystalline structure of the CaO NPs was assessed by XRD using a Rigaku Miniflex 600 instrument. The scan speed was set at 0.02° per step for higher resolution of the diffraction peaks, and the angle range was expanded to 10°–90° 2θ to obtain comprehensive data on the crystalline phases. UV-vis spectra were obtained with a Jasco V160 UV-vis spectrophotometer, after dissolving 0.1 mg of CaO NPs in 2 mL of distilled water, to determine the optical properties. The bandgap energy (E.g.,) was computed using the Tauc equation with n fixed at 2, and the UV-vis parameters were adjusted to extend the wavelength range to 200–800 nm, ensuring better detection of absorption edges. FTIR spectra were acquired using a Nicolet iS50 FTIR spectrometer and the KBr technique, with optimized sample-to-KBr ratio (1:100) to enhance signal clarity. The elemental composition, shape, and size of the CaO NPs were analyzed using Field Emission Scanning Electron Microscopy (FE-SEM, Leo Supra 55-Zeiss Inc., Germany), with magnification increased up to ×100,000 for detailed imaging. To assess thermal stability, the CaO NPs were subjected to thermogravimetric analysis using a Mettler-Toledo AG instrument, with heating from room temperature to 900°C at a controlled rate of 10 C/min, and the system was maintained at 900°C for 2 h to ensure complete $CaCO_3$ decomposition. Cooling was performed at 10 C/min to stabilize the material properties.

2.4 Antibacterial assays

The antibacterial activity of eggshells and CaO NPs was evaluated using the well-agar diffusion method. Four bacterial strains were used: *P. aeruginosa* (ATCC 27853), *K. pneumoniae* (ATCC 13883), *E. coli* (ATCC 25922), and *S. aureus* (ATCC 25923). Sample solutions were prepared at concentrations of 0.5, 1, 2, and 3 mg mL^{-1} in DMSO and Mueller-Hinton agar served as growth medium. Bacterial strains were cultured on agar plates at 37°C for 24 h. Then, 6-mm wells were created in the agar and 50 µL of the compound solutions (at different concentrations) was added to each well. The antibacterial activity was compared to that of CIP-5, used as reference. After incubation at 37°C for 24 h, the zones of inhibition were measured. To ensure reliability and consistency, experiments were carried out in triplicate.

2.5 Anticandidal activity

Candida albicans (ATCC 14053) was obtained from the Pasteur Institute of Algiers, Algeria, and cultured on Sabouraud dextrose agar (SDA) plates at 37°C for 48 h. The suspension turbidity was adjusted to the desired cell density (0.5 McFarland standard) using the DensiChek Densitometer from Biomérieux®. To assess the antifungal activities of the samples, *C. albicans* (ATCC 14053) was prepared in SDA using the same method employed for the antibacterial activity evaluation, using the well diffusion technique (Abadi & Abdul-Hussein Mejbel, 2020; Nabila and Putra, 2020; Singh et al., 2020). To calculate the percentage of inhibition of *Candida albicans* (ATCC 14053) using the well diffusion technique, you can use the following formula Equation 1:

$$\text{Percentage of Inhibition} = \left(\frac{\text{D control} - \text{D sample}}{\text{D control}}\right) \times 100 \quad (1)$$

Where: D control is the diameter of the zone of inhibition for the control (no antifungal agent) and D sample is the diameter of the zone of inhibition for the sample (with antifungal agent).

2.6 Heavy metal removal by adsorption

The influence of the following experimental parameters on heavy metal removal was investigated: stirring time (from 0 to 70 min), pH (2-11), CaO NPs amount (from 5 to 40 mg per 100 mL), and temperature (25°C, 35°C, and 45°C). The desired pH values were obtained by NaOH and HCl solutions. For each test, a 50 mL solution containing metal ions (Pd^{2+}, Cr^{2+}, Cd^{2+}, Hg^{2+}) and a known quantity of CaO NPs (the adsorbent) was placed in a 100 mL beaker. The mixture was stirred with a continuous stream of air bubbles (as CO_2 source) at 250 rpm for a specific time to achieve the adsorption equilibrium and facilitate $CaCO_3$ formation at room temperature. At specific time points, the solutions were separated from the CaO NPs by filtration using Whatman filter papers. The removal efficiency (%) and adsorption capacity (mg/L) of the different metal ions was calculated using the following Equations 2, 3:

$$\text{Removal efficiency } (\%) = \left(\frac{(C_0 - C_e)}{C_0}\right) \times 100 \quad (2)$$

$$\text{Adsorption capacity } (\text{mg/L}) = \left(\frac{(C_0 - C_e) \times V}{m}\right) \quad (3)$$

where: C_0 is the initial concentration (ppm) of various metal ions, C_e represents the residual concentration (ppm) and V (L) is the solution volume of heavy metal ions, m (g) is the mass of the CaO NPs.

3 Results and discussion

3.1 Morphological and elemental composition

CaO NPs were synthesized from chicken eggshells (Figure 1) by thermal calcination at 700°C for 7 h to obtain the complete decomposition of $CaCO_3$ and organic matters present in the eggshells (Kumari et al., 2023). High-resolution SEM imaging provides crucial insights into the morphology and size distribution of the CaO NPs, allowing for an assessment of the uniformity and quality of the synthesis process. FE-SEM analysis of the CaO NPs revealed a consistently spherical morphology with diameters ranging from 5 to 30 nm (Figure 2). These observations are consistent with findings from (Khine et al., 2022; Kamran et al., 2023), who also reported spherical CaO NPs within similar size ranges. The uniform spherical shape indicates a well-controlled synthesis process and supports the reproducibility of the nanoparticle formation technique used.

SEM-EDX enhances SEM by providing elemental analysis, confirming the presence and relative abundance of key elements in the CaO NPs. EDX identified oxygen (O) and calcium (Ca) in CaO (Figure 2C), with atomic percentages of 47.75% for O and 52.25% for Ca, which correspond to weight percentages of approximately 26.73% for O and 73.27% for Ca. These values are close to the theoretical 1:1 atomic ratio for CaO. No other elements were detected beyond Ca and *O. Minor* carbon contamination, likely due to CaO's hygroscopic nature, which allows it to absorb water and CO_2 from the air, may affect the EDX analysis. Together, SEM and EDX analyses confirm the successful synthesis and appropriate composition of the CaO NPs, validating their potential effectiveness for various applications (Khine et al., 2022).

3.2 Crystalline structure

XRD diffraction patterns provides crucial insights into the polymorph and size distribution of the CaO NPs. XRD spectra (Figure 3) demonstrated the distinctive characteristics of CaO NPs. Prominent peaks were observed at 18.12°, 28.86°, 34.29°, 47.44°, 51.04°, 54.09°, 62.85°, 64.35°, 67.51°, and 71.92°, indicative of the presence of CaO NPs (JCPDS Card No. 00-037-1497). The Miller indices corresponding to these peaks are as follows: (111) for 18.12°, (200) for 28.86°, (211) for 34.29°, (220) for 47.44°, (310) for 51.04°, (222) for 54.09°, (400) for 62.85°, (331) for 64.35°, (420) for 67.51°, and (422) for 71.92°. These findings are in agreement with previous studies by Bharathiraja et al. (2018), Ramli et al. (2019), and Yazıcılar et al. (2021). The Debye–Scherrer equation, $D = k\lambda/\beta\cos\theta$, was used to estimate the average particle size, where D is the particle size (nm), λ is the wavelength of X-ray radiation (1.5406 Å), k is a constant (0.94), β is the full width at half maximum of the diffraction peak (FWHM), and θ is the Bragg's angle. The average particle size of the CaO NPs was estimated to be approximately 20 nm. This measurement of crystallite size supports the nanostructured nature of the material. Notably, this size is in good agreement with the particle diameters observed via FE-SEM, which ranged from 5 to 30 nm. The close match between the XRD-derived crystallite size and the SEM particle size suggests that the CaO NPs are likely single crystals or possess single-crystal characteristics. These findings highlight the successful production of high-quality CaO NPs, which is crucial for ensuring their effectiveness in various applications.

3.3 UV-vis spectra and bandgap

UV-Vis spectra were recorded for both grinded eggshells and CaO nanoparticles (CaO NPs) dispersed in water, spanning a wavelength range of 200–800 nm. Figure 4A shows the spectra before calcination (grinded eggshells) and after calcination (CaO NPs). The pre-combustion spectra of eggshells exhibit a peak from 250 nm extending to 200 nm, indicative of $CaCO_3$ and related to the electronic transitions and vibrational modes of carbonate ions (CO_3^{2-}). After calcination, the UV-Vis spectrum of CaO NPs in water shifts to start from 240 nm and extends to 200 nm, likely due to the formation of $Ca(OH)_2$. While bulk CaO has a large band gap and shows minimal UV-Vis absorption, dissolved $Ca(OH)_2$ can

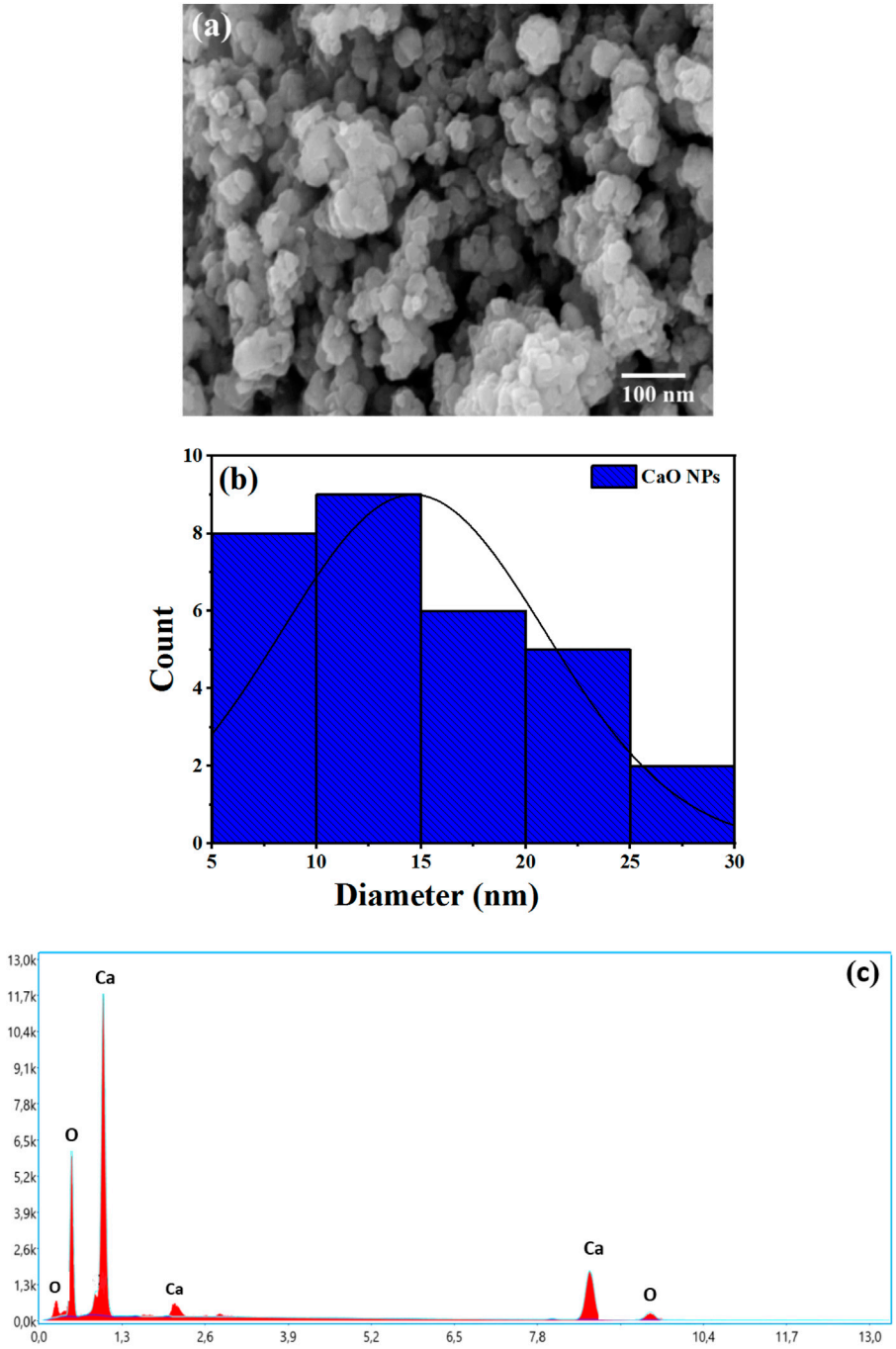

FIGURE 2
FE-SEM analysis of the CaO NPs synthesised from Eggshells: **(A)** SEM images; **(B)** particle size distribution estimated using ImageJ Software and **(C)** EDX analyses.

display weak absorption peaks around 200–240 nm. These observations align with studies by Ikram et al. (2022) and Butt et al. (2015). The bandgap energy of the synthesized CaO NPs (suspension in water) was calculated to be 4.7 eV, determined using the Tauc equation from the plot of $(hv)^2$ versus energy (eV), as shown in Figure 4B. This value is in agreement with previous studies, which report the photonic bandgap of CaO NPs ($CaO/Ca(OH)_4$ in water suspension) to be between 3.5 and 4.9 eV (Lalou and Kadari, 2019).

3.4 Chemical composition and bonding structure

The FTIR spectra before (eggshells) and after calcination (CaO NPs) (Figure 5A) showed that the eggshell sample exhibited a prominent peak at 1395 cm^{-1}, indicative of the high density of eggshell particles and a strong association with carbonate minerals (Carvalho et al., 2011). Additional peaks at ~705 and 874 cm^{-1} further confirmed the presence of $CaCO_3$, corresponding to the in-

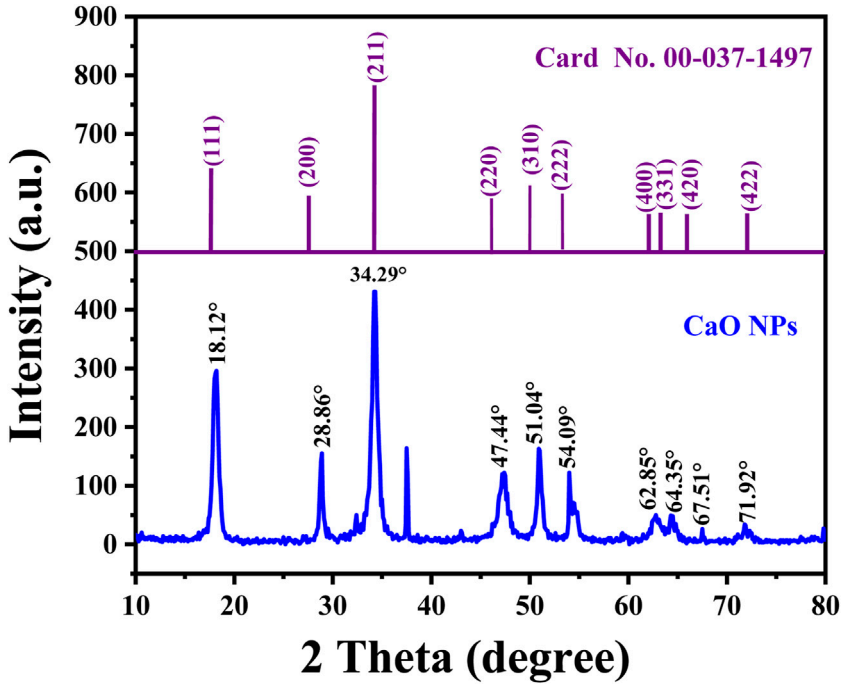

FIGURE 3
XRD patterns of CaO NPs synthesised from Egg shells.

plane and out-of-plane deformation modes (Carvalho et al., 2011). The presence of amines and amides in the eggshell membranes was highlighted by the significant peaks ranging from 3,051 to 3,552 cm^{-1}, 1661 cm^{-1}, and 1395 cm^{-1}, respectively (Carvalho et al., 2011). For CaO NPs, the peak detected at 3,637 cm^{-1} was attributed to the O–H free hydroxyl bond, likely resulting from residual hydroxide or moisture content in the sample (Amor et al., 2023). The sharpness of this peak suggests the formation of particles consisting of a single phase. The additional absorbance bands at ~1600 cm^{-1} and ~800 cm^{-1} confirmed the presence of residual OH groups (Maringgal et al., 2020). The formation of C-O bonds, attributed to CaO NP carbonation, was confirmed by the strong, wide band observed at 1480 cm^{-1} and a peak at 871 cm^{-1} (Atchudan et al., 2022). During calcination, CaO NPs react with air, leading to the generation of CO_2 and H_2O, which are subsequently absorbed onto the CaO surface as free–OH and carbonate species. This indicates the reactivity of surface–OH and lattice oxygen of CaO NPs due to the NP high surface area. Additionally, the minor dips observed in the spectra at 1733 cm^{-1} and 2,533 cm^{-1} were attributed to C–O stretch and CO_2 stretching, respectively (Cavia et al., 2002). The characteristic peak observed at 547 cm^{-1} indicated the Ca–O bond stretch, confirming the presence of chemical residues associated with CaO NP synthesis. Hence, the FTIR analysis provided valuable insights into the chemical composition and structural characteristics of eggshells and CaO NPs.

TGA was employed to analyze mass changes in CaO NPs as a function of temperature under controlled conditions (Figure 5B). A minimal weight reduction of 4.8% was observed in the temperature range of 356°C–385 °C. This weight loss is attributed to the hygroscopic nature of CaO, which absorbs moisture from the atmosphere, rather than the decomposition of residual $CaCO_3$ from the thermal treatment process. The decomposition of $CaCO_3$ typically occurs at temperatures above 550 °C (Barhoum et al., 2015). Since no additional weight loss was detected between 550°C and 700°C, it suggests that the carbonates present in the eggshells had already decomposed during calcination at 700 °C. This minimal mass change confirms the complete transformation of Ca-based materials in the eggshells into CaO, demonstrating the purity, thermal stability, and reliability of the synthesized CaO NPs for various applications.

3.5 Antibacterial activities

Figure 6 and Table 1 show the inhibition zones in the presence of eggshells or the synthesized CaO NPs. When eggshells were used, the inhibition zones against Gram-negative bacteria (*P. aeruginosa*, *K. pneumoniae*, and *E. coli*) increased with the eggshell concentration. For instance, at a concentration of 3 mg mL^{-1}, the inhibition zones ranged from 16 ± 0.2 mm to 17 ± 0.2 mm. Similarly, the inhibition zones against Gram-positive bacteria (*S. aureus*) increased with the eggshell concentration, ranging from 12 ± 0.1 mm to 15 ± 0.1 mm. In the presence of the synthesized CaO NPs, the inhibition zones generally were larger compared with eggshells. At a concentration of 3 mg mL^{-1}, the inhibition zones against Gram-negative bacteria ranged from 18 ± 0.2 mm to 20 ± 0.1 mm and those against Gram-positive bacteria ranged from 16 ± 0.1 mm to 19 ± 0.1 mm. These results indicate an enhancement of the antibacterial activity following the formation of CaO NPs. Comparison with the inhibitory effects of CIP-5 (50 µg) showed that the synthesized CaO NPs exhibited comparable or superior antibacterial activity. Significant differences ($p < 0.05$) were detected

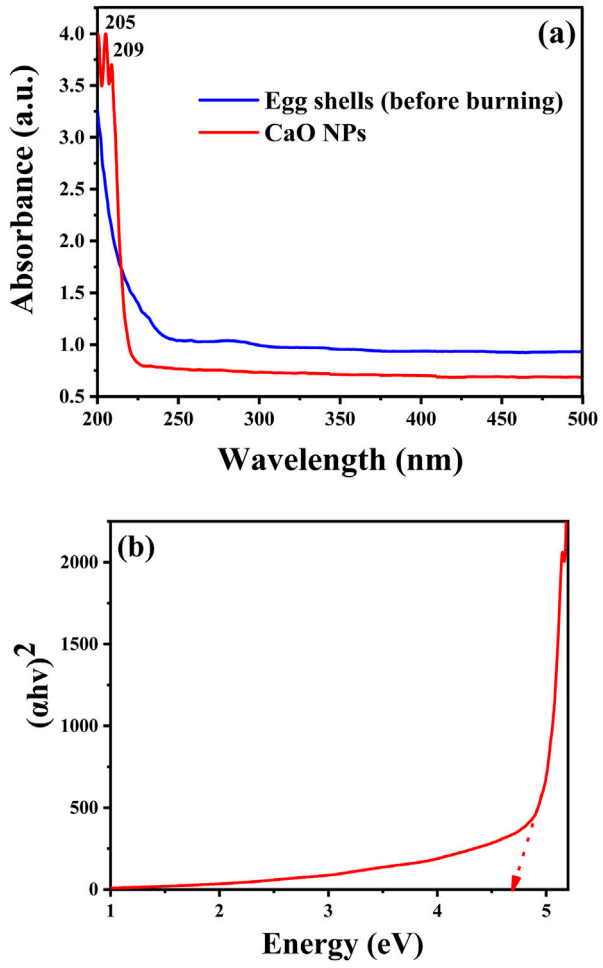

FIGURE 4
Optical properties of eggshells before calcination and the synthesised CaO NPs: **(A)** UV-vis spectra and **(B)** Optical energy bandgap of CaO NPs.

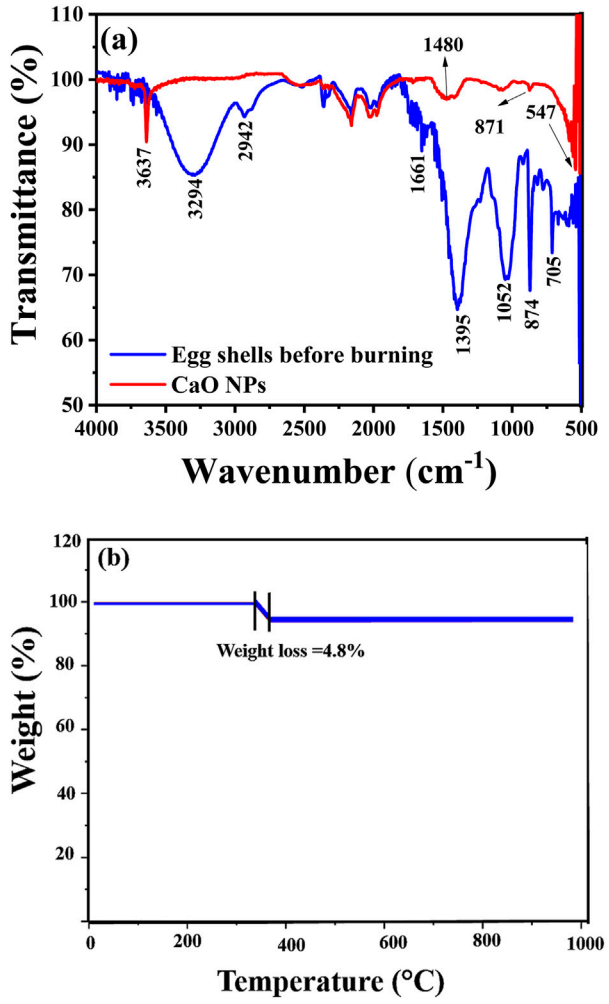

FIGURE 5
Composition of eggshells before calcination and the synthesised CaO NPs: **(A)** FTIR spectra and **(B)** TGA curve of CaO NPs.

between the inhibition zones of different bacterial strains at varying concentrations of CaO NPs. The antibacterial efficacy of the synthesized CaO NPs was statistically superior to that of the raw eggshells across all tested bacterial strains, confirming the enhanced antimicrobial properties of the CaO NPs. For instance, against *P. aeruginosa*, the inhibition zones of CaO NPs (3 mg mL^{-1}) and CIP-5 were 18 ± 0.2 mm and 20 ± 0.1 mm, respectively. These findings are in line with those of previous studies (Alobaidi et al., 2022; Anantharaman et al., 2016; Zaater et al., 2024).

Mina et al. (Carvalho et al., 2011) previously reported an inhibition zone of 15.24 mm for CaO NPs against *E. coli*. Similarly, Alobaidi et al. (2022) observed a positive correlation between CaO NP concentration and inhibition zone diameters, with the largest diameter occurring at 560 µg/mL of CaO NPs against both *S. aureus* and *E. coli*. In various studies, the antimicrobial effectiveness of different materials was assessed against multiple bacterial strains. Chicken eggshells demonstrated a zone of inhibition of 12 mm against *E. coli* (Ismael et al., 2024), and 26.33 mm against *P. aeruginosa* and 33 mm against *E. coli* in another study (Alsohaimi et al., 2020). Carica fruit showed broad-spectrum activity with inhibition zones ranging from 11 to 28 mm across five bacterial species ((Khan et al., 2023). $CaCl_2{\cdot}H_2O$ demonstrated a 28 mm inhibition zone against *E. coli* (Kumar et al., 2021). Shrimp shells and $CaCO_3$ both inhibited *S. aureus* and *E. coli* with inhibition zones of 17–19 mm (Gedda et al., 2015).

In the present study, the antibacterial effectiveness of eggshells and CaO NPs against bacterial strains was compared with that of CaO NPs synthesized using different materials (Table 2).

The enhanced antibacterial activity of CaO NPs compared with eggshells can be attributed to several factors. First, CaO NP synthesis involves the transformation of $CaCO_3$ (present in eggshells) into CaO, resulting in NPs with increased surface area and reactivity. The increased surface area-to-volume ratio of CaO NPs promotes their interaction with bacterial membranes, facilitating their disruption and compromising their integrity, ultimately leading to bacterial cell death. Additionally, upon contact with bacterial cells, CaO NPs can generate reactive oxygen species (ROS) that induce oxidative stress and cause damage to essential biomolecules, further contributing to their antibacterial activity. The alkaline pH environment created by CaO NPs upon dissolution in water disrupts the bacterial homeostasis and metabolic processes, inhibiting bacterial growth

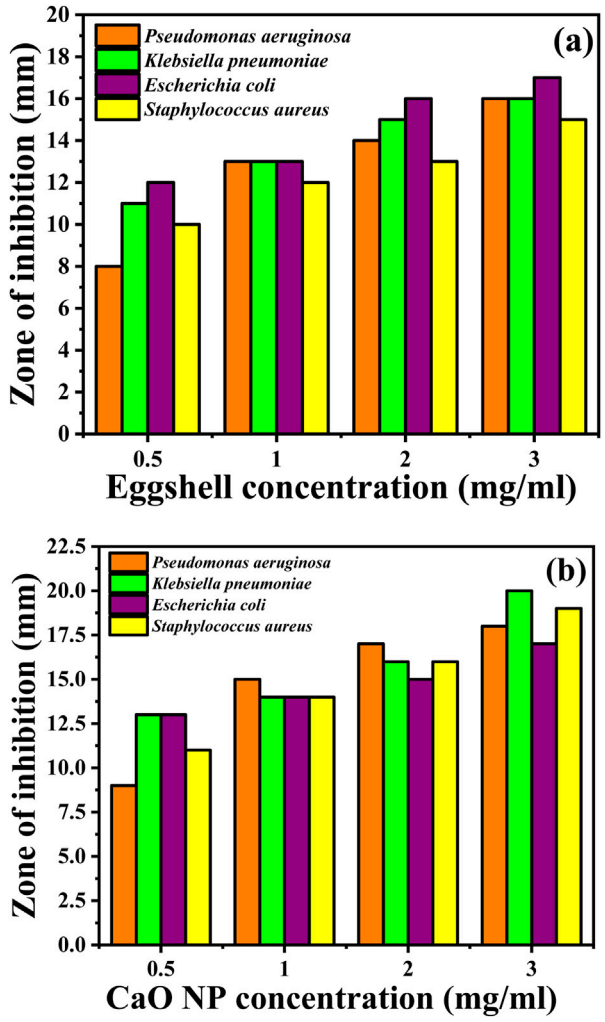

FIGURE 6
Antibacterial activity against the indicated bacteria of **(A)** Eggshells before calcination and **(B)** synthesised CaO NPs.

and survival. Overall, the transformation of eggshells into CaO NPs resulted in NPs with superior antibacterial properties due to their enhanced surface area, reactivity, and ability to generate ROS, making them more effective against a wide range of pathogens.

3.6 Antifungal activity

Percentages of inhibition of *C. albicans* are calculated by comparing the diameter of the inhibition zone (mm) for the control and the sample (mm) using the Agar well diffusion method. Both eggshells and CaO NPs exhibited significant inhibitory effect on *C. albicans* growth after 8 days of incubation (Figures 7A, B; Table 2). Eggshells showed inhibition percentages ranging from 10% to 33% at various concentrations and time points. Higher concentrations led to higher inhibition over time. CaO NPs displayed dose-dependent and time-dependent inhibition of *C. albicans* growth, with inhibition percentages ranging from 15% to 86% across different concentrations and time intervals. CaO NP antifungal activity was higher than that of eggshells, particularly at higher concentrations and longer incubation periods.

The mechanism of *C. albicans* growth inhibition by eggshells and CaO NPs involves several factors (Garcia-Rubio et al., 2020; Han et al., 2023). Eggshells contain $CaCO_3$ that has alkaline properties. The alkaline environment resulting from $CaCO_3$ dissolution disrupts the fungal cell membrane, inhibiting *C. albicans* growth. Additionally, eggshells contain chitinase enzymes that can degrade chitin, a crucial component of fungal cell walls, further compromising *C. albicans* cell integrity. CaO NPs exert antifungal effects through multiple mechanisms. First, CaO NPs have a high surface area-to-volume ratio that facilitates the interaction with the fungal cell membranes, leading to disruption of the lipid bilayer structure and membrane integrity. This is followed by leakage of essential cellular components, leading to fungal cell lysis and death. Second, CaO NPs can generate ROS, such as superoxide radicals (O2•-) and hydroxyl radicals (•OH), upon contact with fungal cells, inducing oxidative stress that damages proteins, DNA, and other essential biomolecules for *C. albicans* survival (Abdal Dayem et al., 2017). Therefore, oxidative stress contributes to inhibiting fungal growth and proliferation.

4 Heavy metal adsorption

Eggshells, primarily composed of $CaCO_3$, have been explored as potential adsorbents for heavy metal removal. However, their effectiveness is limited by several factors. The natural structure of eggshells necessitates extensive grinding to increase surface area and enhance adsorption capacity. Even with such processing, eggshells generally exhibit lower efficiency as adsorbents compared to like CaO NPs. Additionally, the use of eggshells carries the risk of introducing contaminants, such as proteins and other organic waste residues, into the water, which can further complicate the treatment process. The synthesized CaO NPs are highly effective in removing heavy metals such as Pb^{2+}, Cr^{2+}, Cd^{2+}, and Hg^{2+} from water sources due to various adsorption mechanisms including surface complexation, ion exchange, physical adsorption, and precipitation (Alibrahimi and Toamah, 2019; Eddy et al., 2024; Kasirajan et al., 2022). These mechanisms involve distinct chemical interactions and surface properties, which contribute to the efficiency of the adsorption process (see Figure 8).

(1) *Surface Complexation*: Surface complexation occurs when heavy metal ions interact with reactive sites on the CaO NPs surface, such as hydroxyl groups (-OH) or oxygen atoms (-O-). This mechanism can be divided into inner-sphere and outer-sphere complexation. Inner-sphere complexation involves the direct coordination of metal ions to surface groups, forming strong chemical bonds. For example, lead ions (Pb^{2+}) can form inner-sphere complexes with hydroxyl groups on the CaO surface, resulting in the formation of lead (II) hydroxide ($Pb(OH)_2$), which precipitates out of the solution. This reaction is characterized by a high stability constant (log K ~ 6) for the formation of these complexes, indicating strong binding. Outer-sphere complexation, on the other hand, involves weaker electrostatic interactions where water molecules

TABLE 1 Inhibition zones in the presence of eggshells or CaO NPs; the inhibition zone value is the mean value obtained from three separate experiments conducted independently.

Sample	Conc	Zone of inhibition (mm)			
		Gram-negative			Gram-positive
		Pseudomonas aeruginosa	*Klebsiella pneumoniae*	*Escherichia coli*	*Staphylococcus aureus*
Eggshells before burning[a]	0.5 mg mL^{-1}	8 ± 0.2	11 ± 0.1	12 ± 0.1	10 ± 0.1
	1 mg mL^{-1}	13 ± 0.1	13 ± 0.2	13 ± 0.1	12 ± 0.1
	2 mg mL^{-1}	14 ± 0.1	15 ± 0.15	16 ± 0.2	13 ± 0.1
	3 mg mL^{-1}	16 ± 0.2	16 ± 0.1	17 ± 0.2	15 ± 0.1
Eggshells after burning (CaO NPs)[a]	0.5 mg mL^{-1}	9 ± 0.2	13 ± 0.1	13 ± 0.1	11 ± 0.1
	1 mg mL^{-1}	15 ± 0.1	14 ± 0.2	14 ± 0.1	14 ± 0.1
	2 mg mL^{-1}	17 ± 0.1	16 ± 0.2	15 ± 0.2	16 ± 0.1
	3 mg mL^{-1}	18 ± 0.2	20 ± 0.1	17 ± 0.2	19 ± 0.1
Ciprofloxacin	50 µg	20 ± 0.1	22 ± 0.2	19 ± 0.2	21 ± 0.2

[a]DMSO, had no effect on the inhibition zone or antibacterial activity of eggshells and CaO NPs.

TABLE 2 Percentage of *Candida albicans* growth inhibition after incubation with eggshells, CaO NPs at different concentrations, compared to the control (100% growth), for up to 8 days, calculated using the well diffusion technique.

Sample concentration		72 h	96 h	120 h	144 h	168 h	192 h
Eggshells	1 wt%	10	13	18	24	28	33
	5 wt%	19	24	31	37	40	45
	10 wt%	33	54	65	73	76	80
CaO NPs	1 wt%	15	18	23	27	33	42
	5 wt%	23	29	35	39	49	51
	10 wt%	41	60	68	75	81	86

remain between the metal ion and the surface, resulting in less stable adsorption. The small particle size, and high density of reactive sites on CaO NPs enhance these interactions.

(2) Ion Exchange: In ion exchange, metal ions in the aqueous solution replace Ca^{2+} ions on the CaO nanoparticle surface. Heavy metal ions such as Pb^{2+}, Cr^{2+}, Cd^{2+}, and Hg^{2+} can exchange with Ca^{2+} due to their similar ionic radii and charge densities. For instance, Cd^{2+} can effectively replace Ca^{2+} ions on the CaO surface due to their comparable size (Cd^{2+} radius ~0.95 Å vs. Ca^{2+} radius ~1.00 Å) and charge density. The ion exchange process is characterized by a high selectivity for metal ions, with values of selectivity coefficients indicating how favorably different metal ions are exchanged. This mechanism can be particularly effective in removing toxic heavy metals from aqueous solutions, with exchange capacities varying from 1.5 to 3.0 mmol/g depending on the metal ion and CaO surface properties.

(3) Physical Adsorption: Physical adsorption involves the adherence of heavy metal ions to the CaO NP surface through weak van der Waals forces and electrostatic interactions. The small particle size and high surface area of CaO NPs enhance this process by providing more active sites for adsorption. For instance, Pb^{2+}, Cr^{2+}, Cd^{2+}, and Hg^{2+} adhere to the surface of CaO through non-specific interactions. The process is typically reversible due to the weak nature of van der Waals forces, with the adsorption capacity being sensitive to temperature changes.

(4) Precipitation: During precipitation, CaO NPs react with metal ions in the solution to form insoluble metal hydroxides or carbonates. For example, metal ions such as Pb^{2+}, Cr^{2+}, Cd^{2+}, and Hg^{2+} can react with hydroxide ions (OH^-) in the solution to form metal hydroxides like $Pb(OH)_2$, chromium (III) $Cr(OH)_3$, $Cd(OH)_2$, and $Hg(OH)_2$, which precipitate out of the water. Additionally, metal ions can react with carbonate ions (CO_3^{2-}), if present, to form metal carbonates such as $PbCO_3$, $Cr_2(CO_3)$, $CdCO_3$, and $HgCO_3$, which also precipitate and remove the metals from the solution (Kasirajan et al., 2022). The formation of these precipitates is driven by the low solubility products (Ksp) of these compounds. For instance, the solubility product of $Pb(OH)_2$is very low (Ksp ~1.2×10^{-15}), leading to significant precipitation and removal of Pd^{2+} ions from the solution. Similarly, $CdCO_3$ has a low solubility

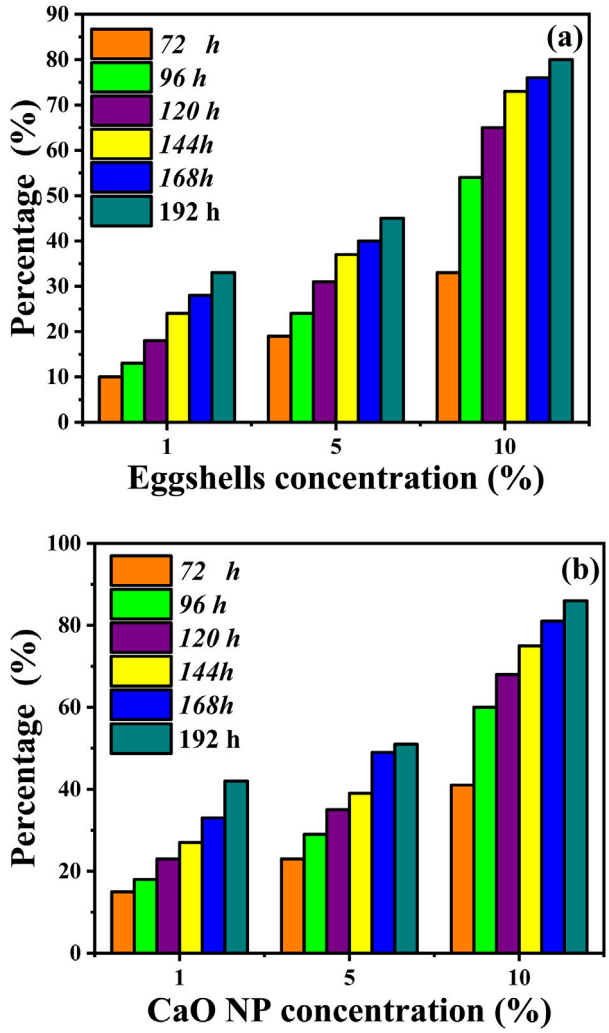

FIGURE 7
Percentage of *Candida albicans* growth inhibition after incubation with eggshells (before calcination) and synthesized CaO NPs, compared to the control (100% growth). Inhibition was measured using the well diffusion technique based on the diameter of the inhibition zone (mm).

product (Ksp ~8.3 × 10^{-12}), facilitating effective removal of Cd^{2+} ions.

After removal of heavy metals, techniques such as sedimentation, filtration, and centrifugation are employed to separate and remove the metal precipitates from the solution (Banković–Ilić et al., 2017). The residual metal hydroxides and carbonates can be repurposed in industrial applications, such as the production of construction materials. For CaO NPs, regeneration methods like acid washing or thermal regeneration are used to restore the nanoparticles for reuse. Acid washing removes adsorbed metals, while thermal regeneration involves heating the nanoparticles to release the metals. Residual substances, such as metal hydroxides and carbonates, can be incorporated into other processes, thus enhancing sustainability and minimizing environmental impact (Velempini et al., 2023).

4.1 Effect of pH on heavy metal adsorption

Figure 9 illustrates the strong dependence of metal ion adsorption by CaO NPs on the pH of the solution, which affects both the adsorbent's surface properties and the metal ion distribution (Supplementary Tables S1, S2 in Supplementary Material). In the experiment, 30 mg of CaO NPs were exposed to 10 ppm solutions of Pb^{2+}, Cr^{2+}, Cd^{2+}, or Hg^{2+} across a pH range from 2 to 11, with the solutions stirred for 30 min to ensure effective interaction between the adsorbent and the metal ions. The results show that the highest removal efficiency and adsorption capacity were achieved at pH 6 or higher. Specifically, at pH 6, the adsorption capacities were 14.5 mg/L for Cd^{2+}, 13.83 mg/L for Pb^{2+}, 14.5 mg/L for Cr^{2+}, and 13.83 mg/L for Hg^{2+}, with removal efficiencies of 94% for Cd^{2+}, 91% for Pb^{2+}, 89% for Cr^{2+}, and 83% for Hg^{2+}. Conversely, at pH levels below 6, there was a noticeable decline in both removal efficiency and adsorption capacity. For instance, at pH 2, the removal efficiencies were significantly lower: 6.83% for Cd^{2+}, 6.5% for Pb^{2+}, 6.83% for Cr^{2+}, and just 2.33% for Hg^{2+}, with adsorption capacities of 8.67 mg/L for Cd^{2+}, 6.5 mg/L for Pb^{2+}, 6.5 mg/L for Cr^{2+}, and 2.33 mg/L for Hg^{2+}.

The observed differences in metal ion removal efficiency can be attributed to the varying chemical properties of the metal ions and their interactions with the sorbent surface. Mercury (Hg^{2+}) shows lower removal efficiency compared to other ions due to its relatively low electronegativity and larger atomic size, which result in weaker interactions with the sorbent. In contrast, Cr^{2+}, Pb^{2+}, and Cd^{2+}, with their higher electronegativity and smaller atomic sizes, exhibit stronger interactions and thus higher removal efficiencies. Additionally, the speciation and complexation behavior of these ions in aqueous solutions influence their adsorption. For example, Cr and Pb form stable complexes with ligands, enhancing their adsorption, while Cd ions form hydroxyl complexes at higher pH, improving their removal efficiency relative to Hg^{2+}. The removal efficiency decreases in very acidic environments due to increased H^+ ion concentration, which makes the sorbent surface more positively charged and weakens the attraction between the sorbent and metal ions. As pH increases, especially in the range of 6–11, the concentration of H_3O^+ ions decreases, making the CaO NPs surface more negatively charged and available for metal ion binding. At pH values above 8, the removal efficiency remains relatively constant, indicating that pH 6 is optimal for maximizing metal ion uptake. (Cruz-Lopes et al., 2021; Mnasri-Ghnimi and Frini-Srasra, 2019).

4.2 Effect of reaction time on heavy metal adsorption

Figure 10 illustrates the effect of reaction time on the removal of Pb^{2+}, Cd^{2+}, Cr^{2+}, and Hg^{2+} by CaO NPs, showing both recovery

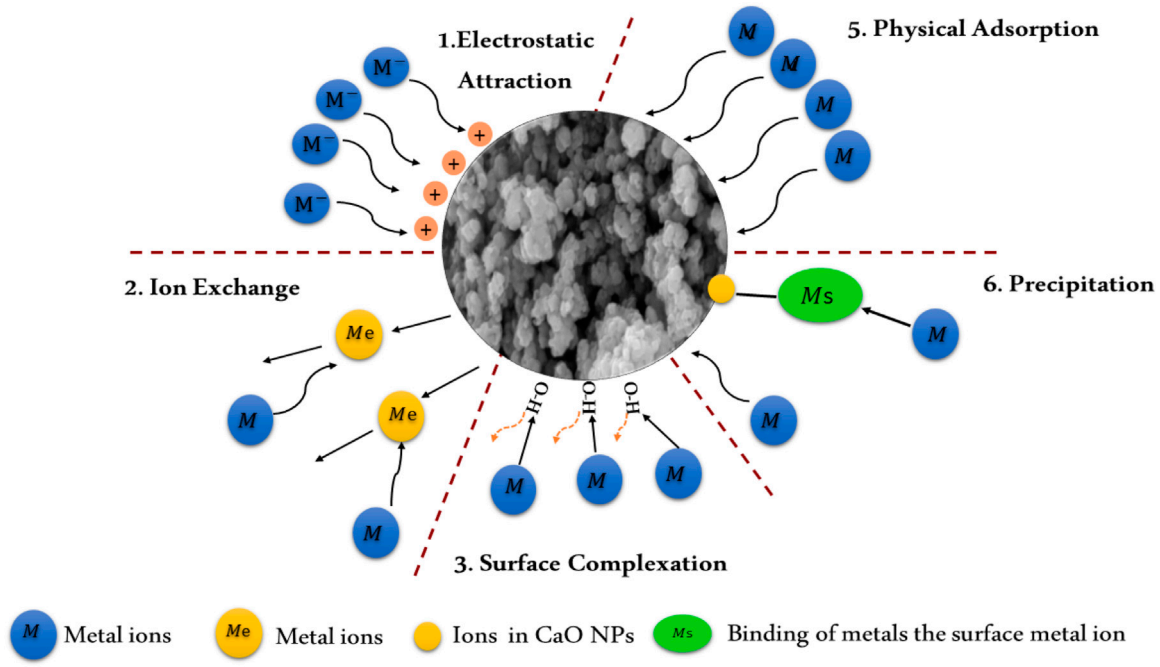

FIGURE 8
Mechanisms of interaction of metal ions with CaO NPs, including surface complexation, ion exchange, physical adsorption, and precipitation, illustrating the removal of heavy metals from aqueous solutions.

percentages and adsorption capacities over various intervals (Supplementary Tables S1, S2 in Supplementary Material). At time zero, no metal ion recovery was observed. After 5 min, the adsorption capacities were 9.17 mg/L for Pb^{2+} and 9 mg/L for Cd^{2+}, while Cr^{2+} and Hg^{2+} had lower capacities of 8 mg/L and 6.33 mg/L, respectively. At 30 min, recoveries had improved significantly, with Pb^{2+} and Cd^{2+} showing adsorption capacities of 16.17 mg/L and 15.67 mg/L, while Cr^{2+} and Hg^{2+} were 15.67 mg/L and 15.17 mg/L. Recovery rates continued to increase, reaching 98% for Pb^{2+} and 97% for Cd^{2+} at 50 min, with adsorption capacities of 16.33 mg/L and 15.83 mg/L, respectively. By 70 min, the maximum recoveries were achieved: 99% for Pb^{2+} and Cr^{2+}, 98% for Cd^{2+}, and 99% for Hg^{2+}, corresponding to the highest adsorption capacities of 16.5 mg/L for Pb^{2+}, 16 mg/L for Cd^{2+}, 16.5 mg/L for Cr^{2+}, and 16.5 mg/L for Hg^{2+}.

These results indicate that extending the reaction time enhances the adsorption efficiency of CaO NPs, allowing for near-complete removal of heavy metal ions. Pb^{2+} and Cr^{2+} achieve higher removal percentages more quickly than Cd^{2+} and Hg^{2+}, reflecting their stronger affinity for the CaO NPs. This rapid saturation is attributed to their smaller ionic radii and higher charge densities, which increase their interactions with the CaO NPs surface. Consequently, Pb^{2+} and Cr^{2+} form more effective bonds, leading to faster binding and higher removal rates. In contrast, Hg^{2+}, although capable of reaching high removal percentages over extended periods, consistently exhibits lower adsorption capacities due to its larger atomic size and lower charge density. This results in weaker interactions with the CaO NPs, requiring more time for Hg^{2+} to approach its maximum removal capacity. These differences highlight how variations in ionic size and charge density influence the rate and effectiveness of metal ion removal (Raji et al., 2023).

4.3 Effect of the adsorbent concentration on heavy metal adsorption

Figure 11 illustrates the impact of CaO NPs concentration on the removal of various metal ions using CaO NPs (Supplementary Tables S1, S2 in Supplementary Material). As the CaO NPs concentration increases, removal efficiency percentages for Pb^{2+}, Cd^{2+}, Cr^{2+}, and Hg^{2+} also rise. At an adsorbent concentration of 5 mg, the removal percentages were 74% for Pb^{2+}, 71% for Cd^{2+}, 70% for Cr^{2+}, and 64% for Hg^{2+}, with corresponding adsorption capacities of 6.83 mg/L for Pb^{2+}, 8.67 mg/L for Cd^{2+}, 6.5 mg/L for Cr^{2+}, and 2.33 mg/L for Hg^{2+}. Increasing the CaO NPs concentration to 30 mg resulted in notable improvements, with removal efficiencies reaching 98% for Pb^{2+} (adsorption capacity of 16.33 mg/L) and Cd^{2+} (16.5 mg/L), and 97% for Cr^{2+} (16.5 mg/L) and Hg^{2+} (16.5 mg/L). However, further increasing the CaO NPs concentration to 40 mg did not significantly enhance the removal efficiency, as the percentages plateaued at 98% for all metal ions. This plateau suggests that, beyond a certain concentration, additional CaO NPs does not lead to significant improvements in removal efficiency, likely due to the saturation of available adsorption sites on the CaO NPs (Hashem et al., 2024).

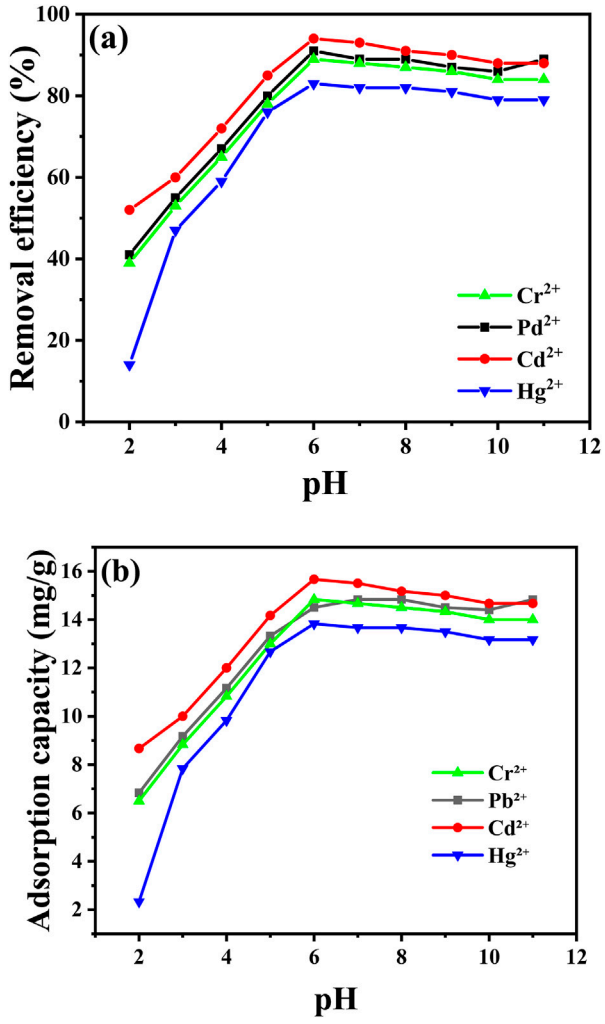

FIGURE 9
Impact of pH (2-11) on removal efficiency **(A)** and adsorption capacity **(B)** of the indicated metal ions at the adjusted conditions (30 min, 25°C, 10 ppm metal ions, 50 mL volume).

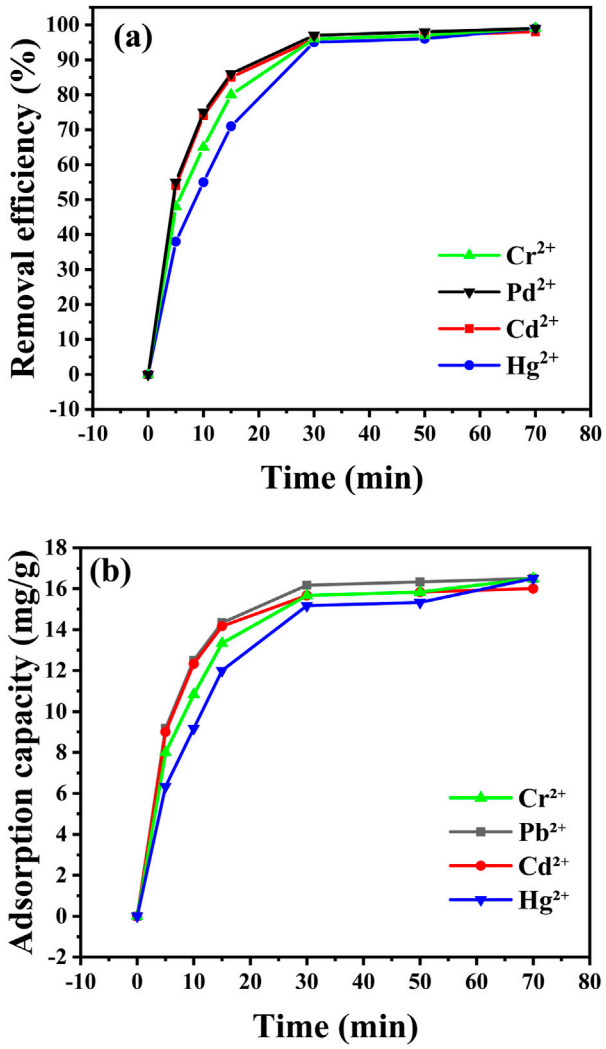

FIGURE 10
Impact of stirring time (from 0 to 70 min) on removal efficiency **(A)** and adsorption capacity **(B)** of the indicated metal ions at conditions (30 mg CaO NPs, pH = 6, 25°C, 10 ppm metal ions, 50 mL volume).

4.4 Effect of temperature on heavy metal adsorption

Effect of temperature on heavy metal adsorption is a critical factor influencing the efficiency of metal ion removal by adsorbents such as CaO NPs. As shown in Figure 12, the removal percentages of Pb^{2+}, Cd^{2+}, Cr^{2+}, and Hg^{2+} by CaO NPs increase with temperature, reaching their maximum values at 45°C (Supplementary Tables S1, S2 in Supplementary Material). At 25°C, the removal rates are 98% for Pb^{2+}, 96% for Cd^{2+}, 97% for Cr^{2+}, and 95% for Hg^{2+}, corresponding to adsorption capacities of approximately 7.8 mg/g, 7.6 mg/g, 7.7 mg/g, and 7.5 mg/g, respectively. The highest removal rates are observed at 45°C, with Pb^{2+}, Cd^{2+}, Cr^{2+}, and Hg^{2+} achieving 99.8%, 99.7%, 99.8%, and 99.5%, respectively, leading to slightly increased adsorption capacities of around 7.9 mg/g for Pb^{2+} and Cr^{2+}, and 7.8 mg/g for Cd^{2+} and Hg^{2+}. The increase in removal efficiency with temperature can be explained by the enhanced kinetics of adsorption and increased mobility of metal ions at higher temperatures. Elevated temperatures typically increase the diffusion rate of metal ions towards the adsorbent surface and can also strengthen the interaction between metal ions and the adsorbent by providing the energy necessary to overcome activation barriers (Kubilay et al., 2007). However, excessively high temperatures might lead to potential desorption of adsorbed metal ions or damage to the adsorbent structure, as noted in various studies (Raji et al., 2023).

The results of these experiments indicate that the conditions for optimal removal of Pb^{2+}, Cr^{2+}, Cd^{2+}, and Hg^{2+}, as summarized in Supplementary Table S1 (supplementary), provide a clear balance between efficiency and practicality. For effective recovery with practical efficiency, 30 min at pH 6 with 40 mg of CaO NPs at 25°C offers a highly effective solution. Under these conditions, the removal rates are 98% for Pb^{2+}, 97% for Cd^{2+}, 97% for Cr^{2+}, and 97% for Hg^{2+}, with corresponding adsorption capacities of approximately 7.84 mg/g for Pb^{2+}, 7.76 mg/g for Cd^{2+}, 7.78 mg/g for Cr^{2+}, and 7.75 mg/g for Hg^{2+}. This approach balances practical

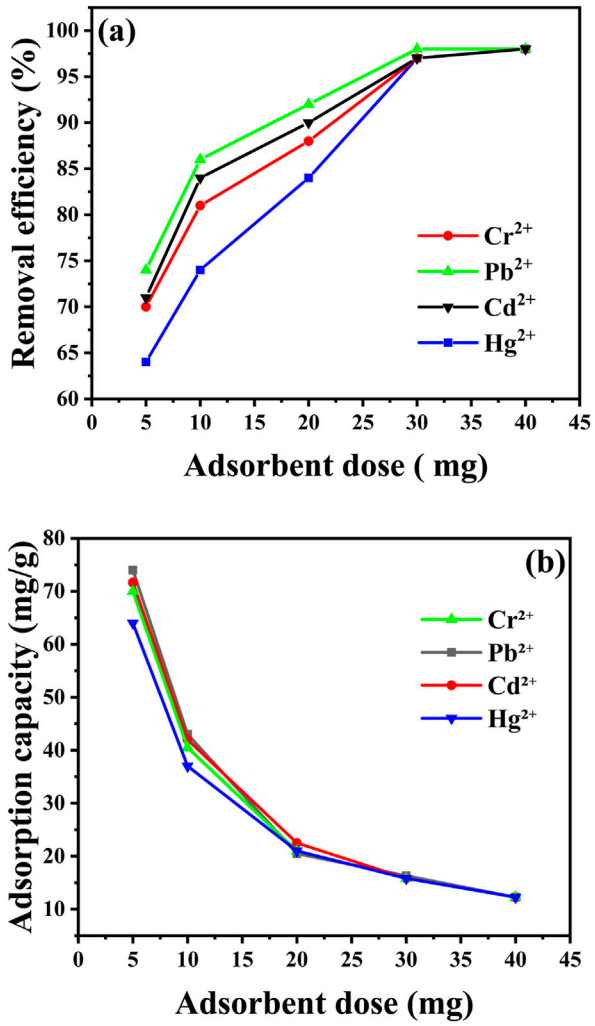

FIGURE 11
Impact of the adsorbent dose (from 5 to 40 mg) on removal efficiency **(A)** and adsorption capacity **(B)** of various metal ions at adjusted conditions (30 min, pH = 6, 25°C, 10 ppm metal ions, 50 mL volume).

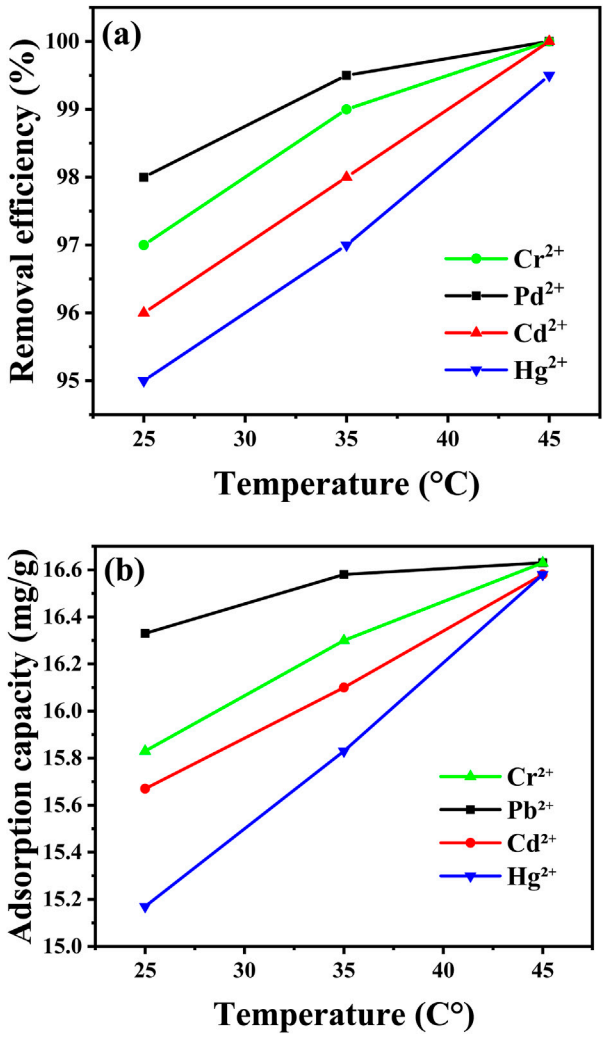

FIGURE 12
Effect of temperature (25°C, 35°C, and 45°C) on removal efficiency **(A)** and adsorption capacity **(B)** of the indicated metal ions at conditions (pH = 6, 10 ppm metal ions, 30 mg of CaO NPs).

considerations of time and cost while delivering substantial metal ion removal. Conversely, if near-complete removal is critical and time or cost is less of a concern, extending the process to 70 min at pH 6 with 40 mg of CaO NPs at 45°C yields the highest removal rates: 99% for Pb^{2+}, 98% for Cd^{2+}, 99% for Cr^{2+}, and 99% for Hg^{2+}, with slightly higher adsorption capacities of around 7.88 mg/g for Pb^{2+}, 7.80 mg/g for Cd^{2+}, 7.82 mg/g for Cr^{2+}, and 7.79 mg/g for Hg^{2+}. While this extended condition achieves nearly complete removal, it involves increased energy consumption and operational costs.

Comparison of the efficacy of CaO NPs derived from different sources (eggshells, $CaCl_2$, and periwinkle shells) for removing various heavy metal ions from aqueous solutions (Table 3) showed that the obtained CaO NPs displayed unique characteristics in terms of size and shape. For instance, CaO NPs derived from eggshells had a crystalline size of 24.34 nm and a spongy appearance, while those from $CaCl_2$ had irregular shapes with a size <100 nm. Similarly, the absorption conditions (pH, stirring time, temperature, and adsorbent dosage) varied among studies. The results show high removal efficiencies of different heavy metal ions (e.g., cadmium, lead, cobalt, and mercury) in specific conditions. The high removal rate (99% using the optimal conditions) obtained with CaO NPs derived from eggshells highlighted their effectiveness in mild conditions. These findings provide valuable insights for the development of efficient and environmentally friendly methods for heavy metal ion removal from aqueous solutions.

5 Conclusion

This study highlights the potential of utilizing chicken eggshells, a common and sustainable waste product, for the eco-friendly synthesis of calcium oxide nanoparticles (CaO NPs). By calcining eggshells at 700°C, we successfully produced spherical, single-crystal CaO NPs with diameters ranging from 5 to 30 nm and a bandgap energy of approximately 4.7 eV. These nanoparticles were thoroughly

TABLE 3 Comparative analysis of metal ion removal using CaO NPs obtained using different CaO sources.

CaO source	CaO NP size and shape	Adsorption conditions	Heavy metal removal	References
Eggshells	24.34 nm	Heavy metal (35, 55 and 75 ppm CdII), volume of 100 mL, (0.25, 0.5, 0.75 and 1.25 g) adsorbent dose, pH (3-9), and time 30 min	99.1% removal achieved at initial 55 ppm Cd (II), pH 7, time of 50 min, 0.75 g adsorbent	Muleta et al. (2024)
$CaCl_2$	Irregular shapes with a size <100 nm	Heavy metal of 10 ppm (Hg2+,Cr2+), volume of 100 mL, 30 g adsorbent dose, pH (2-10), temperature of (64.85, 44.85, 24.85°C and 9.85°C), and time of 5–50 min	100% of Hg^{2+} and Cr^{2+} removal was achieved at an initial 30 mg adsorbent, 30 min stirring, ≈338°C, and pH 7	Toamah and Fadhil (2019)
Eggshells	Crystalline size of 24.34 nm, with a spongy and foamy appearance	Heavy metal of 60–120 ppm Pb-II, volume of xx mL, (0.5, 0.75 and 1 g) adsorbent dose, pH (3-9), and time of 45, 75, and 105 min	99.07% Pd removal was achieved at the initial concentration of 75.46 ppm Pd (II), pH 6.94, 0.838 g adsorbent, and time of 101.97 min	Kasirajan et al. (2022)
$CaCl_2$	Particle size <100 nm	Heavy metal 50–350 ppm Co(II), volume of 100 mL, 0.05 mg adsorbent dose, pH 2-10, temperature of 5, 25, 45°C and 65°C, and time 30 min	99% Co(II) removal was achieved at 50 ppm Co(II), 0.05 mg adsorbent, 30 min, pH 7, and 25°C	Alibrahimi and Toamah (2019)
Periwinkle shells	Crystallite size 18 nm	Heavy metal of 250 ppm Pb2+, volume of 100mL, 0.5 g adsorbent dose, temperature of 45°C, and time of 75 min	80% Pb^{2+} removal achieved at 250 ppm, 0.5 g adsorbent, 75 min and 45°C	Eddy et al. (2024)
Eggshells	Size = 20 nm and spherical morphology	Heavy metal of 60–120 ppm ($Pb2^+$, $Cr2^+$, $Cd2^+$, and $Hg2^+$), volume of 100 mL, (5–40 mg per 100 mL) adsorbent dose, pH (2–11), temperature of 25°C, 35°C and 45°C, and time of 0–70 min	99% for Pb^{2+}, 98% for Cd^{2+}, 99% for Cr^{2+}, and 99% for Hg^{2+} removal achieved at 40 mg adsorbent, 70 min, pH = 6, and 45°C	This study

characterized, demonstrating significant antibacterial activity against *S. aureus*, *K. pneumoniae*, and *E. coli*, as well as effective inhibition of *Candida* albicans. The CaO NPs also exhibited considerable promise in environmental applications, particularly for the removal of heavy metal ions from aqueous solutions. The optimization of key variables—pH, contact time, adsorbent dose, and temperature—revealed that the optimal conditions for metal ion removal were at pH 6, with a contact time of 30 min, 40 mg of CaO NPs, and 25°C. This configuration achieved recovery rates of 98% for Pb^{2+}, 97% for Cd^{2+}, 97% for Cr^{2+}, and 97% for Hg^{2+}, with corresponding adsorption capacities of 16.17 mg/L for Pb^{2+}, 15.67 mg/L for Cd^{2+}, 15.67 mg/L for Cr^{2+}, and 15.17 mg/L for Hg^{2+}. For near-complete removal, extending the process to 70 min at pH 6°C and 45°C resulted in the highest recovery rates: 99% for Pb^{2+}, 98% for Cd^{2+}, 99% for Cr^{2+}, and 99% for Hg^{2+}, with enhanced adsorption capacities of 16.5 mg/L for Pb^{2+}, 16.0 mg/L for Cd^{2+}, 16.5 mg/L for Cr^{2+}, and 16.5 mg/L for Hg^{2+}. However, this enhanced efficiency comes with increased energy consumption and operational costs. Finally, we can conclude that this study offers a sustainable and cost-effective solution for environmental and biomedical challenges, promoting the recycling of waste materials and supporting green nanotechnology.

Data availability statement

The raw data supporting the conclusions of this article will be made available by the authors, without undue reservation.

Author contributions

HH: Writing–original draft, Visualization, Validation, Software, Resources, Methodology, Investigation, Formal Analysis, Data curation, Conceptualization. SZ: Conceptualization, Data curation, Formal Analysis, Investigation, Methodology, Resources, Software, Validation, Visualization, Writing–original draft. IB: Writing–original draft, Visualization, Validation, Software, Resources, Methodology, Investigation, Formal Analysis, Data curation, Conceptualization. AAn: Writing–original draft, Validation, Software, Resources, Methodology, Investigation, Formal Analysis, Data curation, Conceptualization. AT: Writing–original draft, Validation, Software, Methodology, Investigation, Formal Analysis, Data curation, Conceptualization. AAs: Funding acquisition, Project administration, Resources, Validation, Visualization, Writing–review and editing. DC: Writing–review and editing, Visualization, Validation, Resources, Project administration. MB: Visualization, Writing–review and editing, Validation, Supervision, Resources, Project administration, Funding acquisition, Formal Analysis. AB: Writing–review and editing, Writing–original draft, Visualization, Validation, Supervision, Software, Resources, Project administration, Methodology, Investigation, Funding acquisition, Formal Analysis, Data curation, Conceptualization.

Funding

The author(s) declare that financial support was received for the research, authorship, and/or publication of this article. The authors declare that financial support was received for this article's research, authorship, and/or publication. Consortium Author AB and AAl were financially supported by the Science, Technology and Innovation Funding Authority (Project ID 42811) and Researchers Supporting Project number (RSP-2024R78), King Saud University, Riyadh, Saudi Arabia.

Conflict of interest

The authors declare that the research was conducted in the absence of any commercial or financial relationships that could be construed as a potential conflict of interest.

Publisher's note

All claims expressed in this article are solely those of the authors and do not necessarily represent those of their affiliated organizations, or those of the publisher, the editors and the reviewers. Any product that may be evaluated in this article, or claim that may be made by its manufacturer, is not guaranteed or endorsed by the publisher.

Supplementary material

The Supplementary Material for this article can be found online at: https://www.frontiersin.org/articles/10.3389/fenvs.2024.1450485/full#supplementary-material

References

Abadi, A. K., and Abdul-Hussein Mejbel, F. (2020). Study of the effect of antifungal on candida albicans isolated from different cases. *Plant Arch. (09725210)* 20 (1).

Abdal Dayem, A., Hossain, M. K., Lee, S. B., Kim, K., Saha, S. K., Yang, G.-M., et al. (2017). The role of reactive oxygen species (ROS) in the biological activities of metallic nanoparticles. *Int. J. Mol. Sci.* 18 (1), 120. doi:10.3390/ijms18010120

Abuzeid, H. M., Julien, C. M., Zhu, L., and Hashem, A. M. (2023). Green synthesis of nanoparticles and their energy storage, environmental, and biomedical applications. *Crystals* 13 (11), 1576. doi:10.3390/cryst13111576

Aditya, S., Stephen, J., and Radhakrishnan, M. (2021). Utilization of eggshell waste in calcium-fortified foods and other industrial applications: a review. *Trends Food Sci. & Technol.* 115, 422–432. doi:10.1016/j.tifs.2021.06.047

Alibrahimi, A. A., and Toamah, W. (2019). Removing metal ions of cobalt (II) from aqueous solutions by CaO nanoparticle. *J. Phys. Conf. Ser.* 1279, 012023. doi:10.1088/1742-6596/1279/1/012023

Alobaidi, Y. M., Ali, M. M., and Mohammed, A. M. (2022). Synthesis of calcium oxide nanoparticles from waste eggshell by thermal decomposition and their applications. *Jordan J. Biol. Sci.* 15 (2). doi:10.54319/jjbs/150215

Alsohaimi, I. H., Nassar, A. M., Elnasr, T. A. S., and amar Cheba, B. (2020). A novel composite silver nanoparticles loaded calcium oxide stemming from egg shell recycling: a potent photocatalytic and antibacterial activities. *J. Clean. Prod.* 248, 119274. doi:10.1016/j.jclepro.2019.119274

Amor, I. B., Hemmami, H., Laouini, S. E., Temam, H. B., Zaoui, H., and Barhoum, A. (2023). Biosynthesis MgO and ZnO nanoparticles using chitosan extracted from Pimelia Payraudi Latreille for antibacterial applications. *World J. Microbiol. Biotechnol.* 39 (1), 19. doi:10.1007/s11274-022-03464-5

Anantharaman, A., Ramalakshmi, S., and George, M. (2016). Green synthesis of calcium oxide nanoparticles and its applications. *Int. J. Eng. Res. Appl.* 6 (10), 27–31.

Andarini, N., Farida, R. S., and Haryati, T. (2021). The effect of different precursor concentration on the synthesis of CaO nanoparticles with coprecipitation methods for palm oil transesterification catalysis. *Reaktor* 21 (2), 45–51. doi:10.14710/reaktor.21.2.45-51

Atchudan, R., Perumal, S., Joo, J., and Lee, Y. R. (2022). Synthesis and characterization of monodispersed spherical calcium oxide and calcium carbonate nanoparticles via simple pyrolysis. *Nanomaterials* 12 (14), 2424. doi:10.3390/nano12142424

Boey, P.-L., Maniam, G. P., and Abd Hamid, S. (2011). Performance of calcium oxide as a heterogeneous catalyst in biodiesel production: A review. *Chem. Enginee. J.* 168 (1), 15–22. doi:10.1016/j.cej.2011.01.009

Banković–Ilić, I. B., Miladinović, M. R., Stamenković, O. S., and Veljković, V. B. (2017). Application of nano CaO–based catalysts in biodiesel synthesis. *Renew. Sustain. Energy Rev.* 72, 746–760. doi:10.1016/j.rser.2017.01.076

Barhoum, A., Van Assche, G., Makhlouf, A. S. H., Terryn, H., Baert, K., Delplancke, M.-P., et al. (2015). A green, simple chemical route for the synthesis of pure nanocalcite crystals. *Cryst. Growth & Des.* 15 (2), 573–580. doi:10.1021/cg501121t

Bharathiraja, B., Sutha, M., Sowndarya, K., Chandran, M., Yuvaraj, D., and Praveen Kumar, R. (2018). Calcium oxide nanoparticles as an effective filtration aid for purification of vehicle gas exhaust. *Adv. Intern. Combust. Engine Res.*, 181–192. doi:10.1007/978-981-10-7575-9_9

Butt, A., Ejaz, S., Baron, J., Ikram, M., and Ali, S. (2015). CaO nanoparticles as a potential drug delivery agent for biomedical applications. *Dig. J. Nanomater. & Biostructures (DJNB)* 10 (3).

Chen, Q., Luo, Z., Hills, C., Xue, G., and Tyrer, M. (2009). Precipitation of heavy metals from wastewater using simulated flue gas: sequent additions of fly ash, lime and carbon dioxide. *Water Resea.* 43 (10), 2605–2614. doi:10.1016/j.watres.2009.03.007

Carvalho, J., Araújo, J., and Castro, F. (2011). Alternative low-cost adsorbent for water and wastewater decontamination derived from eggshell waste: an overview. *Waste Biomass Valorization* 2, 157–167. doi:10.1007/s12649-010-9058-y

Cavia, M., Fernandez-Muino, M., Gömez-Alonso, E., Montes-Pérez, M., Huidobro, J., and Sancho, M. (2002). Evolution of fructose and glucose in honey over one year: influence of induced granulation. *Food Chem.* 78 (2), 157–161. doi:10.1016/s0308-8146(01)00393-4

Cruz-Lopes, L. P., Macena, M., Esteves, B., and Guiné, R. P. (2021). Ideal pH for the adsorption of metal ions Cr6+, Ni2+, Pb2+ in aqueous solution with different adsorbent materials. *Open Agric.* 6 (1), 115–123. doi:10.1515/opag-2021-0225

Eddy, N. O., Garg, R., Ukpe, R. A., Ameh, P. O., Garg, R., Runde, M., et al. (2024). Application of periwinkle shell for the synthesis of calcium oxide nanoparticles and in the remediation of Pb2+-contaminated water. *Biomass Convers. Biorefinery*, 1–19. doi:10.1007/s13399-024-05285-y

Ferdoush, M. R., Al Aziz, R., Karmaker, C. L., Debnath, B., Limon, M. H., and Bari, A. M. (2024). Unraveling the challenges of waste-to-energy transition in emerging economies: implications for sustainability. *Innovation Green Dev.* 3 (2), 100121. doi:10.1016/j.igd.2023.100121

Garcia-Rubio, R., de Oliveira, H. C., Rivera, J., and Trevijano-Contador, N. (2020). The fungal cell wall: Candida, Cryptococcus, and Aspergillus species. *Front. Microbiol.* 10, 2993. doi:10.3389/fmicb.2019.02993

Gedda, G., Pandey, S., Lin, Y.-C., and Wu, H.-F. (2015). Antibacterial effect of calcium oxide nano-plates fabricated from shrimp shells. *Green Chem.* 17 (6), 3276–3280. doi:10.1039/c5gc00615e

Han, C., Chen, Y., Shi, L., Chen, H., Li, L., Ning, Z., et al. (2023). Advances in eggshell membrane separation and solubilization technologies. *Front. Veterinary Sci.* 10, 1116126. doi:10.3389/fvets.2023.1116126

Hashem, A., Aniagor, C. O., Farag, S., Fikry, M., Aly, A., and Amr, A. (2024). Evaluation of the adsorption capacity of surfactant-modified biomass in an aqueous acid blue 193 system. *Waste Manag. Bull.* 2 (1), 172–183. doi:10.1016/j.wmb.2024.01.004

Ikram, M., Muhammad Khan, A., Haider, A., Haider, J., Naz, S., Ul-Hamid, A., et al. (2022). Facile synthesis of La-and chitosan-doped CaO nanoparticles and their evaluation for catalytic and antimicrobial potential with molecular docking studies. *ACS omega* 7 (32), 28459–28470. doi:10.1021/acsomega.2c02790

Ismael, E., Fahim, K. M., Ghorab, S. M., Hamouda, R. H., Rady, A. M., Zaki, M. M., et al. (2024) Sustainable recycling of poultry eggshell waste for the synthesis of calcium oxide nanoparticles and evaluating its antibacterial potency against food-borne pathogens.

Kataki, S., Chatterjee, S., Vairale, M. G., Sharma, S., and Dwivedi, S. K. (2021). Concerns and strategies for wastewater treatment during COVID-19 pandemic to stop plausible transmission. *Resources, Conservation and Recycling.* 164, 105156. doi:10.1016/j.resconrec.2020.105156

Kamran, U., Jamal, H., Siddiqui, M. I. H., and Park, S.-J. (2023). Surfactant-capped silver-doped calcium oxide nanocomposite: efficient sorbents for rapid lithium uptake and recovery from aqueous media. *Water* 15 (19), 3368. doi:10.3390/w15193368

Kasirajan, R., Bekele, A., and Girma, E. (2022). Adsorption of lead (Pb-II) using CaO-NPs synthesized by solgel process from hen eggshell: response surface methodology for modeling, optimization and kinetic studies. *South Afr. J. Chem. Eng.* 40 (1), 209–229. doi:10.1016/j.sajce.2022.03.008

Khan, A. U., Hussain, T., Abdullah, Khan, M. A., Almostafa, M. M., Younis, N. S., et al. (2023). Antibacterial and antibiofilm activity of Ficus carica-mediated calcium oxide (CaONPs) phyto-nanoparticles. *Molecules* 28 (14), 5553. doi:10.3390/molecules28145553

Khine, E. E., Koncz-Horvath, D., Kristaly, F., Ferenczi, T., Karacs, G., Baumli, P., et al. (2022). Synthesis and characterization of calcium oxide nanoparticles for CO2 capture. *J. Nanoparticle Res.* 24 (7), 139. doi:10.1007/s11051-022-05518-z

Kubilay, Ş., Gürkan, R., Savran, A., and Şahan, T. (2007). Removal of Cu (II), Zn (II) and Co (II) ions from aqueous solutions by adsorption onto natural bentonite. *Adsorption* 13, 41–51. doi:10.1007/s10450-007-9003-y

Kumar, S., Sharma, V., Pradhan, J. K., Sharma, S. K., Singh, P., and Sharma, J. K. (2021). Structural, optical and antibacterial response of CaO nanoparticles synthesized via direct precipitation technique. *Nano Biomed. & Eng.* 13 (2). doi:10.5101/nbe.v13i2.p172-178

Kumari, S., Raturi, S., Kulshrestha, S., Chauhan, K., Dhingra, S., András, K., et al. (2023). A comprehensive review on various techniques used for synthesizing nanoparticles. *J. Mater. Res. Technol.* 27, 1739–1763. doi:10.1016/j.jmrt.2023.09.291

Lalou, N., and Kadari, A. (2019). Influence of Li 2+ doping on the structural and optical properties of CaO synthesized by sol–gel process. *J. Mol. Eng. Mater.* 7 (01n02), 1950002. doi:10.1142/s2251237319500023

Maringgal, B., Hashim, N., Tawakkal, I. S. M. A., Hamzah, M. H., and Mohamed, M. T. M. (2020). Biosynthesis of CaO nanoparticles using Trigona sp. Honey: physicochemical characterization, antifungal activity, and cytotoxicity properties. *J. Mater. Res. Technol.* 9 (5), 11756–11768. doi:10.1016/j.jmrt.2020.08.054

Mnasri-Ghnimi, S., and Frini-Srasra, N. (2019). Removal of heavy metals from aqueous solutions by adsorption using single and mixed pillared clays. *Appl. Clay Sci.* 179, 105151. doi:10.1016/j.clay.2019.105151

Muleta, W. S., Denboba, S. M., and Bayu, A. B. (2024). Corncob-supported calcium oxide nanoparticles from hen eggshells for cadmium (Cd-II) removal from aqueous solutions; Synthesis and characterization. *Heliyon* 10 (6), e27767. doi:10.1016/j.heliyon.2024.e27767

Nabila, V. K., and Putra, I. B. (2020). The effect of Aloe vera ethanol extract on the growth inhibition of Candida albicans. *Med. Glas. (Zenica)* 17 (2), 485–489. doi:10.17392/1098-20

Naz, S., Gul, A., Zia, M., and Javed, R. (2023). Synthesis, biomedical applications, and toxicity of CuO nanoparticles. *Appl. Microbiol. Biotechnol.* 107 (4), 1039–1061. doi:10.1007/s00253-023-12364-z

Perkumienė, D., Atalay, A., Safaa, L., and Grigienė, J. (2023). Sustainable waste management for clean and safe environments in the recreation and tourism sector: a case study of Lithuania, Turkey and Morocco. *Recycling* 8 (4), 56. doi:10.3390/recycling8040056

Raji, Z., Karim, A., Karam, A., and Khalloufi, S. (2023). *Adsorption of heavy metals: mechanisms, kinetics, and applications of various adsorbents in wastewater remediation—a review,* Waste. MDPI. Available at: https://www.mdpi.com/2813-0391/1/3/46.

Ramli, M., Rossani, R. B., Nadia, Y., Darmawan, T. B., Febriani, S., and Ismail, Y. S. (2019) "Nanoparticle fabrication of calcium oxide (CaO) mediated by the extract of red dragon fruit peels (Hylocereus Polyrhizus) and its application as inorganic–anti-microorganism materials," in *IOP conference series: materials science and engineering*. IOP Publishing. Available at: https://iopscience.iop.org/article/10.1088/1757-899X/509/1/012090.

Roy, A., Gauri, S. S., Bhattacharya, M., and Bhattacharya, J. (2013). Antimicrobial activity of CaO nanoparticles. *J. Biomedi. Nanotec.* 9 (9), 1570–1578. doi:10.1166/jbn.2013.1681

Silva, J. A. (2023). Wastewater treatment and reuse for sustainable water resources management: a systematic literature review. *Sustainability* 15 (14), 10940. doi:10.3390/su151410940

Singh, S., Srivastava, B., Gupta, K., Gupta, N., Singh, R., and Singh, S. (2020). Comparative evaluation of antifungal efficacy of five root canal sealers against clinical isolates of candida albicans: a microbiological study. *Int. J. Clin. Pediatr. Dent.* 13 (2), 119–123. doi:10.5005/jp-journals-10005-1718

Toamah, W. O., and Fadhil, A. K. (2019) "Preparation of nanoparticles from CaO and use it for removal of chromium (II), and mercury (II) from aqueous solutions," in *Journal of physics: conference series*. IOP Publishing. Available at: https://iopscience.iop.org/.

Varjani, S., Shah, A. V., Vyas, S., and Srivastava, V. K. (2021). Processes and prospects on valorizing solid waste for the production of valuable products employing bio-routes: a systematic review. *Chemosphere* 282, 130954. doi:10.1016/j.chemosphere.2021.130954

Velempini, T., Ahamed, M., and Pillay, K. (2023). Heavy-metal spent adsorbents reuse in catalytic, energy and forensic applications-a new approach in reducing secondary pollution associated with adsorption. *Results Chem.* 5, 100901. doi:10.1016/j.rechem.2023.100901

Xiong, S., Bozaghian, M., Lestander, T. A., Samuelsson, R., Hellqvist, S., and Öhman, M. (2017). Calcium oxide as an additive for both conservation and improvement of the combustion properties of energy grass: a preliminary study. *Biomass and Bioenergy.* 99, 1–10. doi:10.1016/j.biombioe.2017.02.010

Yazıcılar, B., Böke, F., Alaylı, A., Nadaroglu, H., Gedikli, S., and Bezirganoglu, I. (2021). *In vitro* effects of CaO nanoparticles on Triticale callus exposed to short and long-term salt stress. *Plant Cell Rep.* 40, 29–42. doi:10.1007/s00299-020-02613-0

Zaater, A., Serhoud, M. O., Ben Amor, I., Zeghoud, S., Hemmami, A., Rebiai, A., et al. (2024). Exploring the potential of a Ephedra alata leaf extract: phytochemical analysis, antioxidant activity, antibacterial properties, and green synthesis of ZnO nanoparticles for photocatalytic degradation of methylene blue. *Front. Chem.* 12, 1367552. doi:10.3389/fchem.2024.1367552

Zhang, M., Gao, M., Yue, S., Zheng, T., Gao, Z., Ma, X., et al. (2018). Global trends and future prospects of food waste research: a bibliometric analysis. *Environ. Sci. Pollut. Res.* 25, 24600–24610. doi:10.1007/s11356-018-2598-6